From tomographic imaging to numerical simulations: an open-source workflow for true morphology mesoscale FE meshes

Hani Cheikh Sleiman, Murilo Henrique Moreira, Alessandro Tengattini, Stefano Dal Pont

RILEM Technical Letters (2023) 8: 158-164
https://doi.org/10.21809/rilemtechlett.2023.184

From tomographic imaging to numerical simulations: an open-source workflow for true morphology mesoscale FE meshes

Hani Cheikh Sleiman[1,2,*], Murilo Henrique Moreira[3], Alessandro Tengattini[4,5], Stefano Dal Pont[4]

[1] Department of Mechanical Engineering, University College London, London, UK
[2] Centre for Computational Medicine, Division of Medicine, University College London, London, UK
[3] Federal University of Sao Carlos, Graduate Program in Materials Science and Engineering (PPGCEM), Rod. Washington Luiz, km 235, 13565-905, São Carlos, SP, Brazil
[4] Université Grenoble Alpes, CNRS, Grenoble INP, 3SR, 38000, Grenoble, France
[5] Institut Laue Langevin, 71 Avenue des Martyrs, 38000 Grenoble, France

Received: 05 September 2023 / Accepted: 30 January 2024 / Published online: 01 March 2024

Abstract

Full-field techniques such as tomography are becoming progressively more central in the study of complex phenomena, in particular where spatiotemporal evolution is crucial, as in moisture transport or crack initiation in porous media. These techniques provide a unique insight in the local process whose quantification allows the improvement of our understanding and of the models describing them. Nevertheless, the model validation can be pushed further by attempting to explicitly represent the heterogeneities and simulate their role in the processes. Once validated, these models can be used to perform "virtual experiments", and overcome the limitations of the experiments (e.g., sample size and number, fine control of the boundary and initial conditions). This study proposes a connection between tomography images and mesoscale models through a workflow that mainly employs open-source tools. This workflow is illustrated through the digitization of a Portland cement concrete sample, stemming from neutron tomographies and resulting in a numerical finite element mesh. The proposed workflow is flexible, allowing for the conversion of images from various sources, such as x-ray or neutron tomographies, to different numerical representations of the domain, such as finite element meshes or even a discrete domain required by discrete element methods, while preserving real morphologies with an accuracy proportionate to the specific need of the problem. Beside its generalizability, our method also offers automated labelling of the different domains and boundaries in both the volumetric and surface meshes, which is often necessary for assigning material properties and boundary conditions. Finally, the series of image, geometry and mesh processing steps described in this work are made available on a GitHub repository.

Keywords: Conformal Meshing; Concrete Mesostructure; Mesoscale Modelling; Neutron Imaging

1 Introduction

Multiscale materials showcase diverse characteristics at various levels of observation, often requiring consideration of multiple scales to comprehensively describe their behavior [1]. Concrete for instance, a subcategory of geomaterials, is considered as a multiscale material due to its complex structure and properties that emerge from interactions across multiple length scales. Three length scales can at least be considered for this material: the microscale, the mesoscale and the macroscale. At the microscale, concrete comprises cement paste, aggregates, and voids, with interactions between cement particles and water, hydration product formation shaping its microstructure. Moving to the mesoscale, elements like aggregate arrangements, pore distribution, the interfacial transition zone (ITZ), micro-cracks play pivotal roles. At the macroscale, concrete's properties, including compressive and tensile strength, elasticity, and thermal behavior, emerge from the cumulative effects of micro and mesoscale structures and their interactions.

Many studies in the literature highlight the role of mesostructure on the overall behavior of concrete undergoing different types of loading. Those studies especially emphasize the role of strain incompatibilities between the cement matrix and the aggregates on mechanical behavior [2], micro-cracks formation [3], failure mechanisms [4, 5] damage under fire accidents [6], the effect of cracks on the local permeability [7], *etc*. Besides experimental evidence, mathematical models developed at the mesoscale are of a great benefit to enhance the predictive capacity of numerical approaches. In fact, most of the models at the macroscale display a complex mathematical formulation to describe the averaged energy, mass, and momentum transfer of a homogenized material. Mesoscale models are useful, not only to simulate processes at the mesoscale, but also to help parameterize and validate

*Corresponding authors: Hani Cheikh Sleiman, e-mail: h.sleiman@ucl.ac.uk

macroscale models. This can be done either by simple calibration or by use of sophisticated upscaling and homogenization techniques [8, 9]. In addition, mesoscale models can also be used to propose phenomenological behavior laws that capture the impact of local processes [10].

It follows that mesoscopic models require a non-homogeneous material field and that the generated mesh should account for multiple domains. In addition to the homogenized mortar phase (accounting for the sand fines and cement paste), other domains could be added such as aggregates, macro-pores, ITZ, *etc*. It should be noted that the impact of the explicit representation of some of the domains is still disputed in the literature and is highly dependent on the type of physics to be modelled. For instance, while the ITZ may play an important role in mechanical simulation, its relevance in certain moisture transfer contexts may be deemed negligible [11]. In addition, there is no agreement on how to model this domain (zero-thickness cohesive element) or what thickness should be attributed to it [12, 13].

Previous studies at the mesoscale suggest different methods to build the required multi-domain mesh. In [14], the generated mesostructure of the aggregates consisted of diameter-varying disks/spheres and their variation followed an experimental particle size distribution curve, thus respecting the volume fraction of aggregates in the concrete volume. However, the simplification in the aggregates shape overlooks the influence of their true morphology. In addition, no explicit modeling of the ITZ is considered despite its proven effect on the failure mechanism in mechanical simulations. In [15], a THM model is introduced featuring spherical aggregates and a weak interface transition zone (ITZ) to simulate concrete behavior. However, neither the particle size distribution nor their shape was accurately accounted for, raising concerns about the model's representativeness in simulating real concrete materials. In [4], a simple and straightforward mapping scheme between a XCT[a]-informed voxelized mesostructure and a regular cubic mesh is proposed. In fact, this approach involves transforming each voxel into eight-noded hexahedral cubic elements. Consequently, directly operating on the initial tomography data is not feasible due to the resulting excessive element count. To address this, compressing the image (scaling it down) becomes necessary in order to decrease the voxel count. However, this compression introduces inaccuracies in representing the volume fractions of the segmented phases, demanding meticulous sensitivity analysis to determine the appropriate compression level. In Stamati et al. [16], a projection-based method of a trinary segmentation of a XCT on a tetrahedral mesh is proposed. The resulting mesh is however non-conformal and results in having shared mesh elements between the different domains. This necessitates non-conventional FE techniques capable of managing strong discontinuities, like the Extended or the Embedded Finite Element Method (XFEM and EFEM, respectively). On the other hand, the formulation of those methods are especially beneficial to predict crack initiation and propagation and can be parameterized with only a few number of parameters easily identified through conventional experiments.

In [10], a fully-coupled meso-scale THM model is proposed to study the effect of a single big aggregate on the overall behaviour of a mortar sample. However, the conformal mesh used in this study was generated between a volume-equivalent ellipsoid and a cylinder since the big aggregate was oval-like shaped. No workflow was therefore proposed by the authors to transition from the tomography to the conformal mesh. Finally, a weakly-coupled THM mesoscale model is proposed in [17] that applied a similar mapping scheme to that in [4], however, this time the mesostructure was obtained after a series of image processing steps applied to the original neutron tomography.

With the increasing number of experiments that employ advanced imaging techniques such as (but not limited to) x-ray and neutron tomography (see for instance the following literature reviews [18, 19, 20] and the following studies at low-temperature [21], moderate temperature [22], high temperature [23, 24, 25] and cracked medium [26], *etc*), there is a need to propose a method that bridges the experimental-numerical gap between complex heterogeneous 3D images obtained by tomography experiments and the 3D morphology-conserving digital representation of such features using multi-domain FE meshes. This work presents two possible pipelines for this purpose (a hybrid, predominantly MATLAB-based approach and a full Python approach). To illustrate that, the step-by-step series of image-processing and computational geometry methods devised on the workflows are applied to a neutron tomography of a concrete sample tomography to obtain a conformal multi-domain mesh that can be used for FE applications.

2 Material and Methods

2.1 General Workflow

The example used in this communication is that of a concrete sample that underwent THM processes while being scanned using x-ray and neutron tomography simultaneously. The concrete mixture is composed of cement, sand, gravels and water. The detailed composition of the sample is described in [22].

The neutron tomography of the concrete sample was acquired at the NeXT-Grenoble beamline [27]. Specifically, 900 projections were acquired over a 360° rotation. All the image acquisition parameters are detailed in [22] and the data can be found at:

https://doi.ill.fr/10.5291/ILL-DATA.UGA-60.

The sets of radiographies were then reconstructed into the corresponding 3D volumes by means of the Feldkamp (FDK) back projection algorithm, as implemented in the commercial software X-act (from RX-solutions).

[a] x-ray Computed Tomography

Besides the aforementioned medianing of the radiographies, some small corrections for beam hardening were also applied during the reconstruction step.

The reconstructed image can be seen as 3D neutron attenuation field where the aggregates have a lower neutron attenuation than the surrounding mortar matrix (cement paste and sand fines which shape is not detectable by the image resolution) due to their distinct water content, as seen in Figure 1a). In fact, water molecules heavily attenuate neutrons due to the presence of Hydrogen element (which has a very strong interaction with neutrons). Therefore, based on the distinct gray value between the aggregates and the surrounding mortar, an intensity-based segmentation is used to separate between these two components.

It should be noted that in the case presented herein, the focus is to obtain a mesh considering only coarser aggregates (with an equivalent spherical radius of 4mm or more, as seen in the particle size distribution curves presented in Figure 1 d), where the sieved image is compared to the original image), hence, the distinction between pores and aggregates is not required, as the former are way smaller than the threshold size. Simultaneous segmentation of the pores and aggregates exist in the literature, such as the multimodal analysis of neutron and x-ray tomographies as obtained in the NeXT equipment, and described by Roubin et al. [28].

The result of this operation is a binary image of the aggregates, as shown in Figure 1 b). However, since the sand and gravels granulometry ranges from fractions of a millimeter to several millimeters, the binary image shows sand particles which shape is represented by a few voxels only. This largely increases the computational cost of the meshing process, as a consequence, discarding small sand fines is needed for practical purposes. A possible solution for this is to use watershed algorithms to label each particle and characterize it by its equivalent spherical radius, as seen in the sequence of Figures 1 c), e) and f). In this study, the specific value of 4mm was chosen somewhat arbitrarily to establish a cutoff. Below this threshold, the aggregates were not treated as separate entities; rather, their collective influence was integrated into the behaviour of the homogenized mortar phase. It is also important to highlight that the accuracy of the method is partly function of the richness of the image of origin. The approach proposed herein is, in this respect, agnostic to the origin of the image (e.g., Neutron, x-ray or magnetic resonance imaging) and its quality. The *required* accuracy is, conversely a function of the specific application, e.g. some first order description of the shape of grains (in the order of tens/hundreds of microns) in granular media seem to be sufficient to capture some of the more salient aspects of the process [29], but a much richer description and smaller scales is known to be needed for crack propagation in crystalline solids. Furthermore, there may be a necessity for a meticulous sensitivity analysis concerning the threshold value in certain scenarios, such as mechanical failure simulations. Additionally, it's imperative to rigorously assign the effective properties of the homogenized phase.

However, as observed by the authors during the analysis, the performance of the watershed algorithm in separating each aggregate individually is not flawless and some small particles can be mistakenly associated to a large particle in some cases. To remove those persistent particles, denoising filters (despeckle filter) or binary operations (a series of erode-dilate operations) can be used.

The next step is to downscale the denoised binary image - resulting in the representation present in Figure 1 g) - and to apply a marching cube algorithm to obtain a surface mesh of the aggregates. A 3D surface smoothing algorithm is then applied to smooth the voxelized morphology of the aggregates, as depicted in Figure 1 h). Additional processing steps can sometimes be required in order to fix the surface mesh (in case it is not watertight, or it presents intersecting shells problems or even if it requires remeshing, *etc*).

Finally, the aggregates surface mesh can be imported to a capable meshing software or library to generate the multi-domain tetrahedral mesh, as shown in Figure 1 i). A labelling step of the different mesh surfaces might be needed to assign the boundary conditions of the yet-to-be-solved numerical problem, this can be observed in Figure 1 j).

The full pipeline that includes the different image, geometry and mesh processing steps can be visualized in Figure 1.

2.2 Detailed Workflow 1: Hybrid MATLAB-Python (HMP) approach

This first approach is a hybrid one that uses Python scripts for the preliminary imaging processing of the tomography and for the mesh format conversion, and that relies heavily on a MATLAB toolbox called GIBBON (The Geometry and Image-Based Bioengineering add-On) [30]. GIBBON is an open-source MATLAB toolbox that includes CAD, geometry and image processing tools. This toolbox interfaces free open source softwares such as TetGen [31] that possesses quality meshing capabilities. A MATLAB license is required for this part of the proposed methodology.

After reconstruction, the aggregates and the sand particles are easily distinguishable from their surrounding matrix given their distinct attenuation value (see Figure 1 a)). It follows that applying a simple intensity-based threshold is sufficient to segment the aggregates in the raw image. This operation is basic and can be performed in any software or library with image processing capabilities, resulting in Figure 1 b).

As mentioned in the previous section, the small aggregates which have a sphere-equivalent diameter below an arbitrary value of 4mm for instance are to be removed. This was possible by applying a watershed algorithm [32] which labels individual sand and aggregates particles - shown in Figure 1 c) - and assign a sphere-equivalent diameter to each one of them. In this work, this operation was done using the SPAM Python package [33].

The previous operation, although very effective and capable of removing most of the aggregates below 4mm, allows some small particles to be mistakenly attributed to large particles (see for instance the difference between Figure 1 f) and Figure 1 g) as smaller ones are removed). To get rid of these impurities, multiple denoising filters could be used such as the despeckle filter or by simply applying multiple Erode-Dilate

operations. Multiple softwares and packages provide implementation of such filters and binary operations. In this work, the despeckle filter implementation of ImageJ software [34] was used and was applied multiple times.

The binary image was then downscaled and a Marching Cubes Algorithm [35] was applied on the processed binary image to extract the outer shell of the aggregates. The resulting surface mesh is then smoothed using SurfaceSmooth function [36] from the MATLAB file exchange, leading to the surface mesh shown in Figure 1 h). Alternative functions in GIBBON such as PatchSmooth can also be used for this purpose with two possible smoothing methods (Laplacian or Humphreys-Classes smoothing).

It should be noticed that these algorithms are parametrized enabling thorough control of the process, and thus it may require trial-and-error tests for selecting the appropriate set of parameters to balance the smoothing properly and achieve representative geometries. The complexity of this stage can be also related to the shape of the aggregate as rounded natural ones (such as the ones considered in the example presented in this work) are easier to smooth than artificial grinded raw material with sharp edges.

Once the aggregates surface mesh is smoothed, we create a cylindrical surface mesh and we use the TetGen [31] GIBBON interface to create the multi-domain tetrahedral conformal mesh illustrated by Figure 1 i).

Finally, the mesh can be converted to multiple formats using the meshio library [37].

We note that all of the described steps in this pipeline are available on the GitHub repository at: https://github.com/ANR-MultiFIRE/TomoToFE.

2.3 Detailed Workflow 2: a Python-based approach

The current workflow is proposed as a completely open-source alternative to Workflow 1. It presents the advantage of having all the required steps within a single software, from the tomography image to the finite element mesh. If a Python package is used for the numerical modeling stage, the whole process can be set up on a single reproducible environment. One potential downside when constructing a pipeline using multiple libraries is the possibility of encountering compatibility issues such as namespace collisions or version conflicts. Nevertheless, all the packages herein can operate simultaneously within the same environment without facing any dependency conflicts.

The process starts with the reconstructed tomographies stored as a stack of files .tiff. Due to faster load times and the possibility of compression, the stack is converted to a .npz file based on the NumPy Python library [38]. Next, the same image processing applied in Workflow 1 is applied, starting from the segmentation of the different phases through thresholding the image and following with the labeling of each individual aggregate through the watershed algorithm of [32], shown in Figures 1 b) and 1 c), respectively.

The next step in the workflow is the removal of smaller aggregates that were mistakenly labeled as a part of a larger aggregate (undersegmentation). In order to do so a succession of erode-dilate operations is applied to the image. In the proposed pipeline, the tomography image stored as a NumPy array is cast in a UniformGrid object from the PyVista library [39]. It should be mentioned that the SPAM library or scikit-image [40] can be employed as well; however, as further steps will take advantage of functionalities of PyVista, the current methodology adopts the PyVista implementation of the erosion-dilation process, as a mean to reduce the number of transitions between distinct Python libraries. As a bonus, the PyVista library enables the fast rendering of tridimensional images within the Python integrated development environment (IDE).

Next, with the tomography image comprising only the aggregates whose sizes lie in the range of the mesoscale feature of interest, a marching cubes algorithm is utilized to obtain a surface mesh from the aggregates. It should be noted that because of the PyVista implementation of the marching cubes' algorithm, some aggregates are not watertight, and some holes on the surface mesh of the aggregates are observable. PyVista itself has a functionality that can fill holes, however, depending on the hole size, the surface mesh can be coarse at such regions, which can pose problems in the finite element mesh generation step.

Thus, the PyMeshFix library [41] is used to fill the holes and performing a refinement of the region that is patched. After that, the surface mesh can be recast as PyVista PolyData object and each aggregate can be separated as independent submeshes.

The next stage aims to create .stl files for each aggregate for loading within the Gmsh software [42], this can be done using PyVista, which can also be used for performing surface smoothing on the aggregates. The researcher can choose to either apply a Laplacian smoothing or a method based on Taubin's algorithm, which is the one selected in the current workflow due to its volume-preserving capability, which leads to Figure 1 h). This stage can be optional depending on the features of the structure that is being analyzed. For natural aggregates, for instance, this step is less relevant than for objects containing tubular geometries with sharp corners.

This stage also can highlight the flexibility of the proposed workflow which allows to simply alter the geometry of features of interest, for example to assess the role of one or more heterogeneities in the system, which would be virtually impossible experimentally.

Finally, with all the .stl files from each individual aggregate, Gmsh can be used to create the overall structure of the object, mark the external boundaries, and most importantly, the internal boundaries between matrix and aggregates, and the whole domain can be meshed. Local mesh refinement can be applied with the information on the internal boundaries, resulting in Figure 1 i). This can also be crucial for different numerical models, as it might be required to define constitutive laws that represent the interfacial transition zone between the different phases. Finally, as proposed in Workflow 1, the mesh can be converted to the format required for the numerical method tool of choice, by also using the meshio library [37].

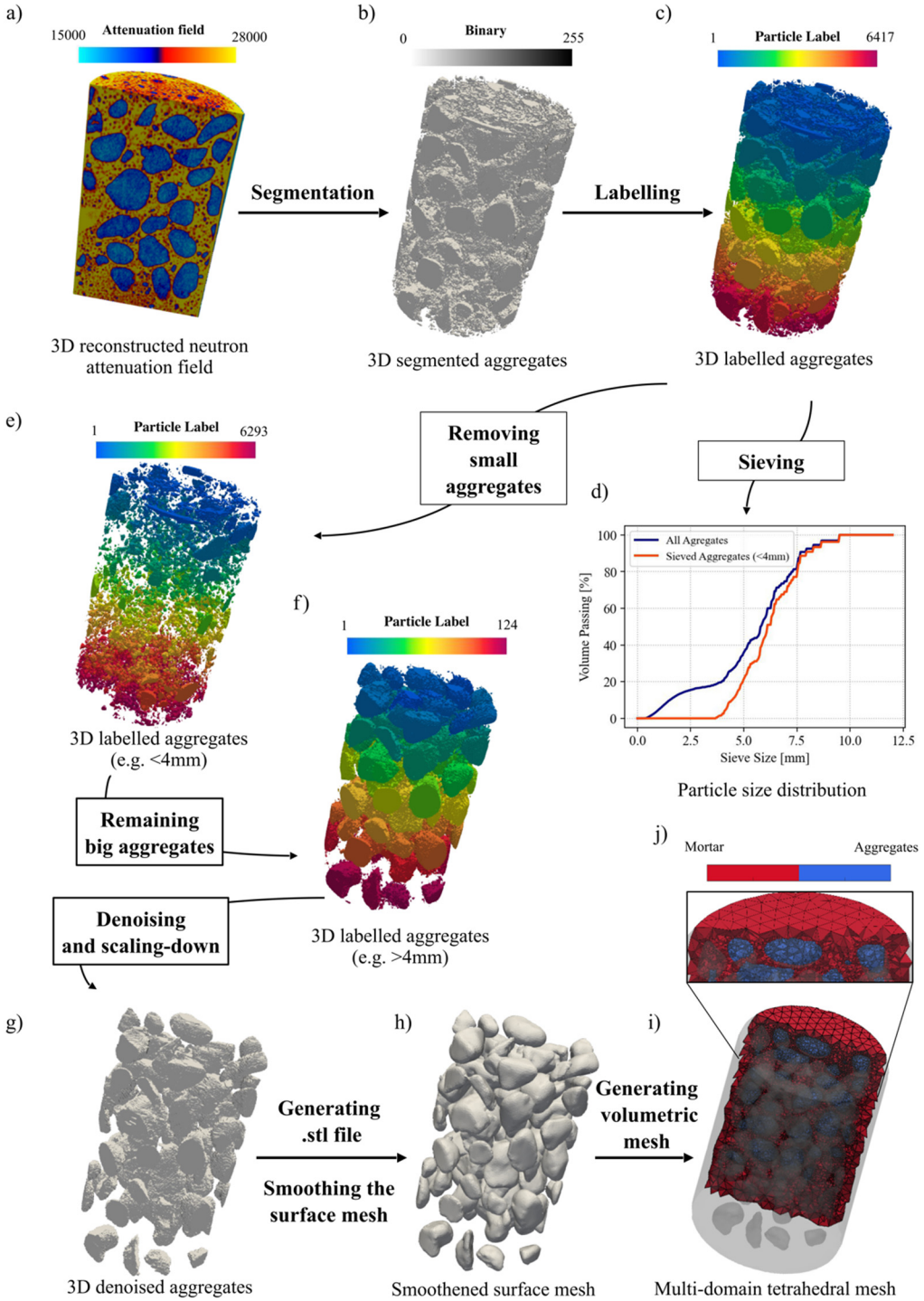

Figure 1. Individual stages of the general workflow, starting from a) the neutron tomography image, b) the segmented phases, c) the labeled aggregates, d) the digital sieving of the aggregates, e) the sieved aggregates larger than 4mm, f) the relabelled image, g) resulting image after erosion-dilation process, h) the surface mesh, and, finally, i) the obtained volumetric mesh with j) the detail of the mortar and aggregates.

3 Conclusions

Heterogeneity plays a crucial role in multiple processes. Nonetheless, traditionally the material response is simulated neglecting this heterogeneity because of a lack of insight in their role as well as to simplify the numerical formulation. Additionally, limitations on available techniques hindered the observation and comprehension of the dynamics of such process *in-situ*.

Currently, though, such context changed, and the current work proposes a streamlined open-source workflow to obtain finite element meshes from tomography images. This setup enables mesoscale analysis on an arbitrary number of features of interest.

The novelty of the methods proposed herein lies on the flexibility and simplicity of the tools, as the same process can be extended to different fields of application, as well as considering different tomography images (such as x-rays instead of neutrons or even the mathematical models that will be used for the simulation of the process, such as both continuum approaches such as FEM, or even the discrete techniques as discrete element modelling – DEM). In the case of DEM, not exemplified in the workflows presented herein, the required representation of the microstructures is achieved by exporting the features of interest (such as the aggregates) in .stl files that can be converted and imported by the simulation software. This enables the creation of assemblies comprising spherical particles of equivalent volume, achievable through standard DEM techniques, or the utilization of aggregates reflecting their authentic morphology, possible in the scope of more sophisticated DEM techniques. Finally, all the code is documented and available at GitHub for the reader (https://github.com/ANR-MultiFIRE/TomoToFE), making its adoption by anyone readily available regardless of their level of expertise in the fields of imaging and numerical simulations, which previously posed a complex learning curve for such analysis.

4 Supplementary Code

The supplementary code for the workflows can be found in the following GitHub repository:
https://github.com/ANR-MultiFIRE/TomoToFE,

while the considered data can be found at:

https://doi.ill.fr/10.5291/ILL-DATA.UGA-60.

Acknowledgments

The authors acknowledge the support of the French *Agence Nationale de la Recherche* (ANR) (project MULTI-FIRE ANR-23-CE51-0001-01) and the Coordenação de Aperfeiçoamento de Pessoal de Nível Superior - Brasil (CAPES) – Finance Code 001. The authors would like to thank the Fundação de Amparo à Pesquisa do Estado de São Paulo - FAPESP (grant numbers: 2021/002510 and 2022/12406-0). The authors are also grateful for the funding from Cancer Research UK (CRUK C44767/A29458).

Authorship statement (CRediT)

Hani Cheikh Sleiman: Conceptualization, Methodology, Software, Investigation, Data curation, Visualization, Writing – original draft

Murilo Henrique Moreira: Methodology, Software, Data curation, Writing – original draft

Alessandro Tengattini: Resources, Validation, Writing – review & editing

Stefano Dal Pont: Conceptualization, Investigation, Supervision, Validation, Writing – review & editing

References

[1] W. D. Callister, D. G. Rethwisch, et al., Materials science and engineering: an introduction, volume 7, John Wiley & Sons New York, 2007.

[2] Z. Kammouna, M. Briffaut, Y. Malecot, Mesoscopic simulations of concrete strains incompatibilities under high creep stress level and consequences on the mechanical properties, European Journal of Environmental and Civil Engineering 23 (2017) 879-893. https://doi.org/10.1080/19648189.2017.1320235

[3] L. Li, Y. Jin, Y. Jia, T. Rougelot, N. Burlion, J. Shao, Influence of inclusion rigidity on shrinkage induced micro-cracking of cementitious materials, Cement and Concrete Composites 114 (2020) 103773. https://doi.org/10.1016/j.cemconcomp.2020.103773

[4] Y. Huang, Z. Yang, W. Ren, G. Liu, C. Zhang, 3D meso-scale fracture modelling and validation of concrete based on in-situ x-ray computed tomography images using damage plasticity model, International Journal of Solids and Structures 67-68 (2015) 340-352. https://doi.org/10.1016/j.ijsolstr.2015.05.002

[5] O. Stamati, E. Roubin, E. Andò, Y. Malecot, P. Charrier, Fracturing process of micro-concrete under uniaxial and triaxial compression: Insights from in-situ x-ray mechanical tests, Cement and Concrete Research 149 (2021) 106578. https://doi.org/10.1016/j.cemconres.2021.106578

[6] M. Moreira, S. Dal Pont, R. Ausas, T. Cunha, A. Luz, V. Pandolfelli, Direct comparison of multi and single-phase models depicting the drying process of refractory castables, Open Ceramics 6 (2021) 100111. https://doi.org/10.1016/j.oceram.2021.100111

[7] M. E. E. Dandachy, M. Briffaut, F. Dufour, S. Dal Pont, An original semi-discrete approach to assess gas conductivity of concrete structures, International Journal for Numerical and Analytical Methods in Geomechanics 41 (2016) 940-956. https://doi.org/10.1002/nag.2655

[8] W. G. Gray, C. T. Miller, Introduction to the Thermodynamically Constrained Averaging Theory for Porous Medium Systems, Springer International Publishing, 2014. https://doi.org/10.1007/978-3-319-04010-3

[9] J. Eliáš, G. Cusatis, Homogenization of discrete mesoscale model of concrete for coupled mass transport and mechanics by asymptotic expansion, Journal of the Mechanics and Physics of Solids 167 (2022) 105010. https://doi.org/10.1016/j.jmps.2022.105010

[10] D. Dauti, S. Dal Pont, M. Briffaut, B. Weber, Modeling of 3D moisture distribution in heated concrete: From continuum towards mesoscopic approach, International Journal of Heat and Mass Transfer 134 (2019) 1137-1152. https://doi.org/10.1016/j.ijheatmasstransfer.2019.02.017

[11] L. E. Dalton, J. M. LaManna, S. Jones, M. Pour-Ghaz, Does ITZ influence moisture transport in concrete?, Transport in Porous Media 144 (2022) 623-639. https://doi.org/10.1007/s11242-022-01826-z

[12] J. Wang, X. Li, A. P. Jivkov, Q. Li, D. L. Engelberg, Interfacial transition zones in concrete meso-scale models - Balancing physical realism and computational efficiency, Construction and Building Materials 293 (2021) 123332. https://doi.org/10.1016/j.conbuildmat.2021.123332

[13] M. Maleki, I. Rasoolan, A. Khajehdezfuly, A. P. Jivkov, On the effect of ITZ thickness in meso-scale models of concrete, Construction and Building Materials 258 (2020) 119639. https://doi.org/10.1016/j.conbuildmat.2020.119639

[14] T. Nguyen, Apport de la modélisation mésoscopique dans la prédiction des écoulements dans les ouvrages en béton fissuré en conditions d'accident grave, Ph.D. thesis, L'Université de Pau et des Pays de l'Adour, 2010.

[15] G. Xotta, G. Mazzucco, V. Salomoni, C. Majorana, K. Willam, Composite behavior of concrete materials under high temperatures, Interna-tional Journal of Solids and Structures 64-65 (2015) 86-99. https://doi.org/10.1016/j.ijsolstr.2015.03.016
[16] O. Stamati, E. Roubin, E. Andò, Y. Malecot, Tensile failure of micro-concrete: from mechanical tests to FE meso-model with the help of x-ray tomography, Meccanica 54 (2018) 707-722. https://doi.org/10.1007/s11012-018-0917-0
[17] H. Cheikh Sleiman, Insights into thermo-hydro-mechanical (THM) behavior of cementitious materials by means of simultaneous neutron/x- ray tomography and 3d mesoscopic modeling., Academic Journal of Civil Engineering (2021) Vol 39 No 1 (2021): Special Issue-RUGC 2021.
[18] E. Perfect, C.-L. Cheng, M. Kang, H. Bilheux, J. Lamanna, M. Gragg, D. Wright, Neutron imaging of hydrogen-rich fluids in geomaterials and engineered porous media: A review, Earth-Science Reviews 129 (2014)120-135. https://doi.org/10.1016/j.earscirev.2013.11.012
[19] P. Zhang, F. H. Wittmann, P. Lura, H. S. Müller, S. Han, T. Zhao, Application of neutron imaging to investigate fundamental aspects of durability of cement-based materials: A review, Cement and Concrete Research 108 (2018) 152-166. https://doi.org/10.1016/j.cemconres.2018.03.003
[20] A. Tengattini, N. Lenoir, E. Andò, G. Viggiani, Neutron imaging for geomechanics: A review, Geomechanics for Energy and the Environment (2020) 100206. https://doi.org/10.1016/j.gete.2020.100206
[21] H. Cheikh Sleiman, A. Tengattini, M. Briffaut, B. Huet, S. Dal Pont, Drying of mortar at ambient temperature studied using high resolution neutron tomography and numerical modeling, Cement and Concrete Composites 131 (2022) 104586. https://doi.org/10.1016/j.cemconcomp.2022.104586
[22] H. Cheikh Sleiman, A. Tengattini, M. Briffaut, B. Huet, S. Dal Pont, Simultaneous x-ray and neutron 4D tomographic study of drying-driven hydro-mechanical behavior of cement-based materials at moderate temperatures, Cement and Concrete Research 147 (2021) 106503. https://doi.org/10.1016/j.cemconres.2021.106503
[23] D. Dauti, A. Tengattini, S. Dal Pont, N. Toropovs, M. Briffaut, B. Weber, Analysis of moisture migration in concrete at high temperature through in-situ neutron tomography, Cement and Concrete Research 111 (2018) 41-55. https://doi.org/10.1016/j.cemconres.2018.06.010
[24] A. Tengattini, S. Dal Pont, H. C. Sleiman, F. Kisuka, M. Briffaut, Quantification of evolving moisture profiles in concrete samples subjected to temperature gradient by means of rapid neutron tomography: Influence of boundary conditions, hygro-thermal loading history and spalling mitigation additives, Strain 56 (2020). https://doi.org/10.1111/str.12371
[25] M. H. Moreira, S. Dal Pont, A. Tengattini, A. P. Luz, V. C. Pandolfelli, Experimental proof of moisture clog through neutron tomography in a porous medium under truly one-directional drying, Journal of the American Ceramic Society 105 (2022) 3534-3543. https://doi.org/10.1111/jace.18297
[26] R. Gupta, B. Lukić, A. Tengattini, F. Dufour, M. Briffaut, Experimental characterisation of transient condensed water vapour migration through cracked concrete as revealed by neutron and x-ray imaging: Effect of initial saturation, Cement and Concrete Research 162 (2022) 106987. https://doi.org/10.1016/j.cemconres.2022.106987
[27] A. Tengattini, N. Lenoir, E. Andò, B. Giroud, D. Atkins, J. Beaucour, G. Viggiani, NeXT-grenoble, the neutron and x-ray tomograph in Grenoble, Nuclear Instruments and Methods in Physics Research Section A: Accelerators, Spectrometers, Detectors and Associated Equipment 968 (2020) 163939. https://doi.org/10.1016/j.nima.2020.163939
[28] E. Roubin, E. Ando, S. Roux, The colours of concrete as seen by x rays and neutrons, Cement and Concrete Composites 104 (2019) 103336. https://doi.org/10.1016/j.cemconcomp.2019.103336
[29] R. Kawamoto, E. Andò, G. Viggiani, J. E. Andrade, All you need is shape: Predicting shear banding in sand with LS-DEM. Journal of the Mechanics and Physics of Solids 111 (2018) 375-392. https://doi.org/10.1016/j.jmps.2017.10.003
[30] K. M. Moerman, GIBBON: The geometry and image-based bioengineering add-on, The Journal of Open Source Software 3 (2018) 506. The MathWorks Inc., Natick, Massachusetts, 2022. https://doi.org/10.21105/joss.00506
[31] H. Si, TetGen, a delaunay-based quality tetrahedral mesh generator, ACMTransactions on Mathematical Software 41 (2015) 1-36. https://doi.org/10.1145/2629697
[32] R. Beare, G. Lehmann, The watershed transform in ITK-discussion and new developments., Technical Report, The Insight Journal, 2006. https://doi.org/10.54294/lf8u75
[33] O. Stamati, et al., spam: Software for practical analysis of materials, Journal of Open Source Software 5 (2020) 2286. https://doi.org/10.21105/joss.02286
[34] J. Schindelin, I. Arganda-Carreras, E. Frise, Fiji: an open-source platform for biological-image analysis, nature methods 9 (2012) 676-682. https://doi.org/10.1038/nmeth.2019
[35] W. E. Lorensen, H. E. Cline, Marching cubes: a high resolution 3d surface construction algorithm, Seminal graphics (1998). https://doi.org/10.1145/280811
[36] M. Lalancette, Surfacesmooth, 2023. [MATLAB Central File Exchange. Retrieved June 3, 2023]. https://www.mathworks.com/matlabcentral/fileexchange/45416-surfacesmooth
[37] N. Schlömer, meshio: Tools for mesh files, 2022. https://doi.org/10.5281/zenodo.6346837
[38] C. R. Harris, et al., Array programming with NumPy, Nature 585 (2020) 357-362. https://doi.org/10.1038/s41586-020-2649-2
[39] B. Sullivan, A. Kaszynski, PyVista: 3D plotting and mesh analysis through a streamlined interface for the Visualization Toolkit (VTK), Journal of Open Source Software 4 (2019) 1450. https://doi.org/10.21105/joss.01450
[40] S. van der Walt, et al., The scikit-image contributors, scikit-image: image processing in Python, PeerJ 2 (2014) e453. https://doi.org/10.7717/peerj.453
[41] M. Attene, A lightweight approach to repairing digitized polygon meshes, The visual computer 26 (2010) 1393-1406. https://doi.org/10.1007/s00371-010-0416-3
[42] C. Geuzaine, J.-F. Remacle, Gmsh: A 3-D finite element mesh generator with built-in pre- and post-processing facilities, International Journal for Numerical Methods in Engineering 79 (2009) 1309-1331. https://doi.org/10.1002/nme.2579